Journal of Alloys and Compounds 509 (2011) 5627–5630

Contents lists available at ScienceDirect

Journal of Alloys and Compounds

journal homepage: www.elsevier.com/locate/jallcom

ZnO nanocoral reef grown on porous silicon substrates without catalyst

H.I. Abdulgafour*, F.K.Yam, Z. Hassan, K. AL-Heuseen, M.J. Jawad

School of Physics, University Sains Malaysia 11800 Penang, Malaysia

ARTICLE INFO

Article history:
Received 20 July 2010
Received in revised form 16 February 2011
Accepted 19 February 2011
Available online 24 February 2011

Keywords:
Oxide materials
X-ray diffraction
Crystal structure
ZnO

ABSTRACT

Porous silicon (PS) technology is utilized to grow coral reef-like ZnO nanostructures on the surface of Si substrates with rough morphology. Flower-like aligned ZnO nanorods are also fabricated directly onto the silicon substrates through zinc powder evaporation using a simple thermal evaporation method without a catalyst for comparison. The characteristics of these nanostructures are investigated using field-emission scanning electron microscopy, grazing-angle X-ray diffraction (XRD), and photoluminescence (PL) measurements of structures grown on both Si and porous Si substrates. The texture coefficient obtained from the XRD spectra indicates that the coral reef-like nanostructures are highly oriented on the porous silicon substrate with decreasing nanorods length and diameter from 800–900 nm to 3.5–5.5 μm and from 217–229 nm to 0.6–0.7 μm, respectively. The PL spectra show that for ZnO nanocoral reefs the UV emission shifts slightly towards lower frequency and the intensity increase with the improvement of ZnO crystallization. This non-catalyst growth technique on the rough surface of substrates may have potential applications in the fabrication of nanoelectronic and nanooptical devices.

1. Introduction

The unique optical and electronic properties of semiconductor nanowires or nanotubes have made them crucially interesting for new technologies. These nanostructures are the key element in the development of nanoscale applications. Among the possible semiconductors to be brought to the nanoscale level, zinc oxide (ZnO) is a desirable candidate because it is a semiconductor with a direct and wide band-gap of 3.37 eV at room temperature and a large exciton energy of 60 meV. Nanoporous materials used as a template provide a simple way of obtaining ZnO nanostructures [1,2]. Thus, porous silicon (PS) has opened new possibilities for Si-based integrated circuits due to its remarkable optical and electronic properties. Applications of PS, including visible photoluminescence (PL) at room temperature, highly efficient electroluminescent devices, photo detectors, and surface acoustic wave (SAW) devices, have been previously reported [3–6]. Numerous technologies have been developed to grow ZnO nanostructures on different substrate materials, such as the vapor–liquid–solid (VLS) method for growth on sapphire with Au as the catalyst, electro-deposition for growth on anodic alumina membrane (AAM) templates, and the vapor–solid (VS) method without a catalyst for growth on Si [7–9].

Among the various fabrication methods for ZnO quasi-one-dimensional nanomaterials described in the literature, evaporation and condensation processes are favored for their simplicity, high quality products, and ability to synthesize nanostructures with different morphologies. The simple ZnO thermal evaporation method developed by Wang et al. [10] is considered the most efficient way of achieving a wide range of ZnO nanostructures despite its high temperature requirement of over 1300 °C. This extremely high temperature limits the application of ZnO nanostructures in the field of nanodevice constructions because most nanoscale constructions involve self-organized processes and high temperatures bring more strict command to other building blocks.

The growth of ZnO nanocoral reefs and nanorod arrays through the vapor–solid (VS) mechanism is possible without the use of metal catalyst. However, the mechanism of ZnO aligned growth remains an open question and requires further study. Several proposed mechanisms have been developed, such as constraint of the pores in either mesoporous Si [11] or porous anodic Al [12], van der Waals interactions [13], and effects of DC bias [14].

For comparison purpose, we also demonstrate the growth of ZnO nanostructures on a PS surface and Si at 900 °C without any catalyst under identical growth condition. Large areas of well-aligned coral reef-like ZnO nanostructures on porous Si and flower-like nanorods on Si have been synthesized.

The morphology and structure of the ZnO nanostructures are investigated using field-emission scanning electron microscopy (FESEM), and grazing-angle X-ray diffraction (XRD). The photoluminescence technique is utilized to characterize the optical properties of the nanostructures. These high-quality nanostructures enrich the family of ZnO nanomaterials and may have potential applications in optoelectronics, sensors, and nanoscale mechanics research.

* Corresponding author.
E-mail address: hind_alshaikh@yahoo.com (H.I. Abdulgafour).

0925-8388/$ – see front matter © 2011 Elsevier B.V. All rights reserved.
doi:10.1016/j.jallcom.2011.02.100

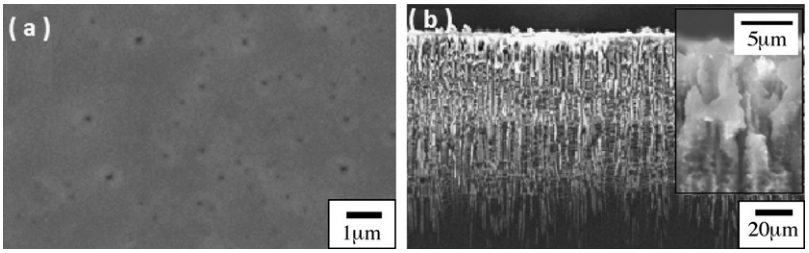

Fig. 1. (a) SEM image of PS sample and (b) SEM crosss section of PS sample prepared at 30 min etching time.

2. Experimental

2.1. Porous Si preparation

Fig. 1 porous Si substrate was fabricated by using n-type Si (1 0 0) wafer through the electrochemical anodization method. In the process, a homemade Teflon cell was used, Si sample and Pt wire were connected as anode and cathode, respectively. The electrolyte was composed of a mixture of 49% aqueous HF and 95% ethanol at a ratio of 1:4 by volume. For the electrochemical etching process, a constant current density of $J = 25\ mA/cm^2$ (supplied by a Keithley 220 programmable current source) was used for 30 min. After etching, the samples were rinsed with deionized water and dried in ambient air.

Fig. 1(a) shows the top-view SEM image of PS sample prepared at 30 min of etching time. For this sample, a uniform distribution of pores around 300 nm has been observed for PS sample prepared at the optimized condition. The porous network was found to be 85 μm as estimated from the SEM cross section as shown in Fig. 1(b). The distribution of the pores is irregular. It also can be regarded as a nanocrystalline skeleton (quantum sponge) immersed in a network of pores. Due to its special structure, porous silicon is characterized by a very large internal surface area that induces a large adsorption, which is another property of the porous silicon [13].

2.2. Synthesis of ZnO nanostructures

The ZnO nanostructures were synthesized in a quartz tube. For growth comparison, a clean n-type Si wafer was placed near to the PS under different surface conditions. The ZnO nanostructures were fabricated on PS and Si substrates using the thermal evaporation process of pure metallic Zn powder (99.9%) without the presence of catalyst. The substrates were placed on top of a ceramic boat with the polished faces aligned toward the Zn powder. The boat was then inserted into the center of a quartz tube furnace. The furnace was heated slowly from 400 to 900 °C under a continuous flow of pure argon and oxygen gases. A constant flow-rate of 350 sccm was maintained for 1 h. After evaporation, the boat was slowly drawn out of the furnace and cooled to room temperature. A white-colored layer formed on the polished face of both PS and Si substrates.

2.3. Characterization

The surface morphology and structure of the ZnO nanostructures were examined by field emission scanning electron microscopy (FE-SEM). The high-resolution X-ray diffractometer (HR-XRD) was used for phase identifications. The PL spectra of the ZnO nanostructures were measured using a He–Cd laser with an excitation wavelength of 325 nm at room temperature.

3. Results and discussion

In our previous work, the controlled self-assembled growth of ZnO nanostructures was obtained by the simple oxidation of Zn powders [6]. This technique yielded large areas of aligned ZnO nanostructures. Fig. 2(a) and (b) shows the entangled and uniform ZnO nanocoral reefs that were formed on the PS substrate, as revealed by FESEM images. The lengths of the nanocoral reefs were 800 nm and had average diameters of about 217 nm with thickness about 6 μm.

For growth on the Si substrate as shown in the highly magnified image in Fig. 3, the average diameters of the nanorods were about 600 nm and their lengths were about 3.5 μm with thickness about 7 μm. As a result, the average diameter of the nanocoral reefs grown on the PS substrate is thinner than that of nanorods grown on the Si substrate, which can be seen by comparing Fig. 2(a) and (b). Obviously the rough surface of substrate plays an important role in controlling the initial stage of ZnO nanostructures formation in the present case.

Zn vapor is condensed easily on the PS surface; and forms a wetting layer. From the SEM images, it can be seen that the ZnO nanocoral reefs on PS substrate was closely connected with the PS substrate. This could be due to the partial filling of the ZnO particles in the pores. Thus, it could improve the structural stability of the porous silicon substrate. Moreover, the distance of the arrays is also beyond the range of van der Waals interaction, so the possible aligned mechanism in our work may be attributed to steric overcrowding [15]. The PS surface had a significant effect on the size and shape of the nanostructures; thus, there was a decrease in the length and size of the nanostructures depending on the roughness of the surface morphology.

Fig. 4 To further understand the influence of morphology differences on the properties of nanostructures, XRD was used to study the crystalline structure and alignment of the products also shows the crystal size in the ZnO films. Fig. 4 shows the typical XRD pattern of the ZnO nanocoral reef and nanorod products on different substrates. All the observed diffraction peaks agreed with

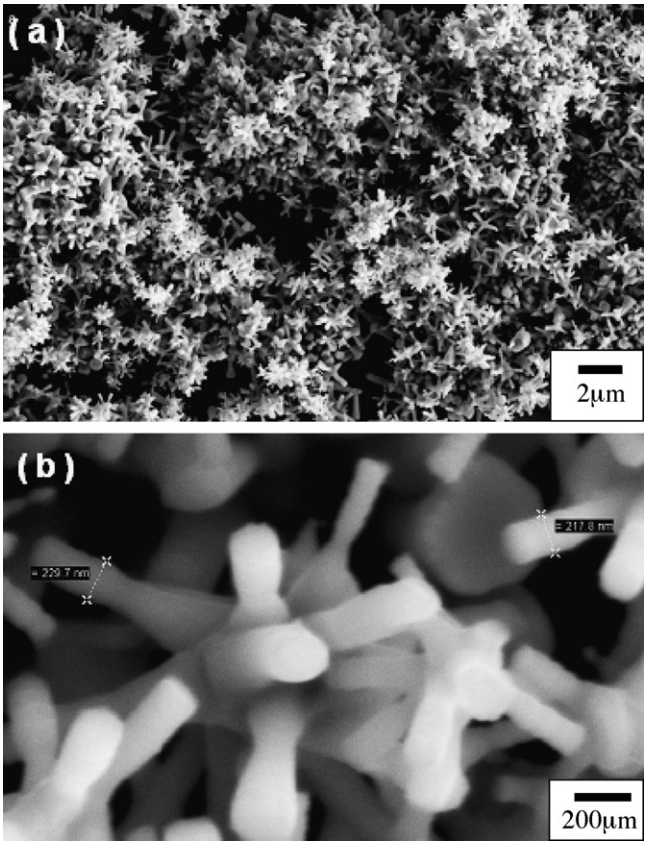

Fig. 2. (a) Low and (b) high magnification SEM images of ZnO nanocoral reef on PS/Si.

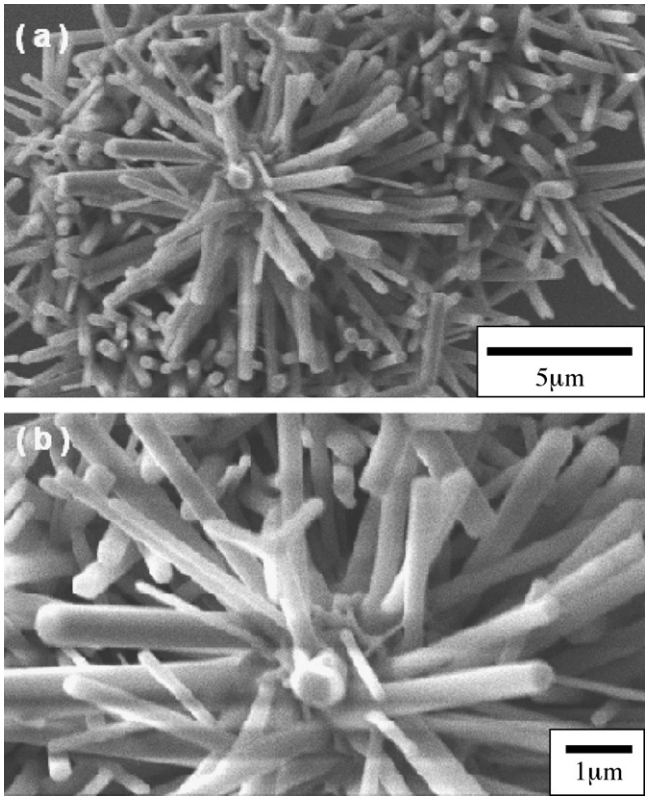

Fig. 3. (a) Low and (b) high magnification SEM images of ZnO nanorods on Si.

the standard card of bulk ZnO with a hexagonal structure (JCPDS No. 800075), the lattice constants of which were $a = 3.249$ Å and $c = 5.206$ Å. No other impurity phase was found. Moreover, the as-grown ZnO nanostructures were polycrystalline in nature with a hexagonal close-packed crystal structure. After oxidizing in air for 1 h, the diffraction patterns of Zn disappeared, and the metallic Zn was transformed completely into ZnO. Several peaks appeared in the spectra of the ZnO films at 2θ from 30° to 65°, corresponding to the (1 0 0), (0 0 2), (1 0 1), (1 0 2), (1 1 0), and (1 0 3) directions of the hexagonal ZnO crystal structure on the different types of surfaces of the PS and Si substrates.

From Fig. 4 one can also see that for the ZnO nanostructures on the porous silicon substrate the intensity of the (0 0 2)-oriented peak (*c*-axis orientation) turn to be higher intensity than on Si substrate. This can be explained in terms of the low surface free energies of the (0 0 2) plane. According to the previous reports

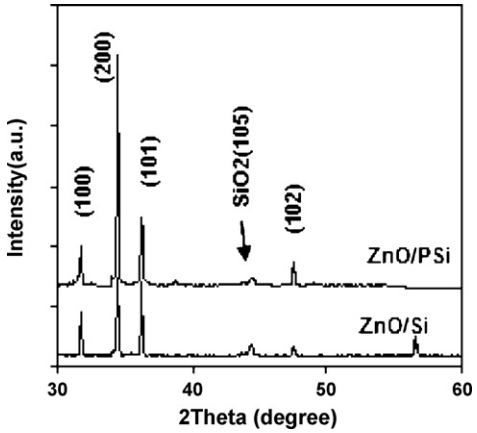

Fig. 4. XRD spectra of ZnO nanostructures grown on PS/Si and Si at 900 °C.

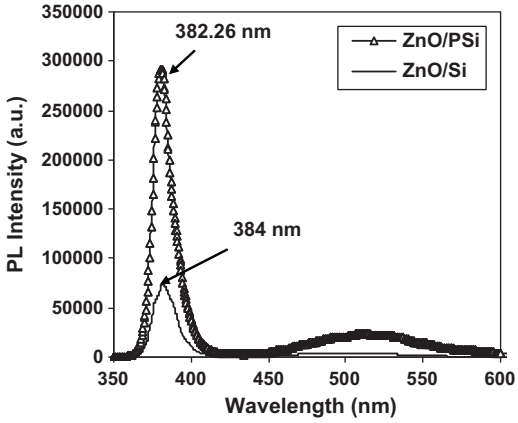

Fig. 5. Room temperature photoluminescence spectra from ZnO nanostructure grown on PS/Si and Si at 900 °C.

[16,17], (0 0 2) was the highest density plane with (0 0 2) the lowest free energy. Furthermore, the strong intensity and narrow width of the ZnO diffraction peaks also indicate that the resulting products had good crystallinity. The (0 0 2) peak at 34.42° was the strongest peak, indicating that the ZnO sample was oriented dominantly along the (0 0 1) growth direction, while peaks at (1 0 0), (1 0 1), (1 0 2), and (1 1 0) indicate that nonepitaxial growth occurred. The average grain size of the ZnO nanostructures can be estimated by the Scherrer formula using the full width at half-maximum (FWHM) value of the XRD diffraction peaks:

$$D = \frac{0.9\lambda}{\beta \cos\theta} \quad (1)$$

where D, λ, θ, and β are the mean grain size, X-ray wavelength of 0.154 nm, Bragg diffraction angle, and the FWHM, respectively. The values of D obtained were about 28 nm for nanocoral reefs on the PS substrate and 42 nm for nanorods on the Si substrates prepared at 900 °C. The values obtained indicate that the pore size of the PS had a significant effect on the mechanism of synthesis of ZnO nanostructures, and could be the initial point of growth of the nanostractures, which starts from the center of the pore and spreads to form the nanoreef. Therefore, the rough surface morphology of the PS substrate plays a major role in controlling the growth of the wetting layer. The porous layer is a good substrate in lattice mismatch heteroepitaxy due to its special surface morphology [18]. The surface of the porous silicon layer is composed of numerous nano-silicon crystals. These nano-silicon crystals maintain (1 0 0) orientation which is planar to the external surface of the Si wafer. These Si crystallites distributed randomly over the entire surface would act as nucleation sites, which induced ZnO nanostructures to grow along the preferred orientation.

Fig. 5 shows the room temperature PL spectra of ZnO nanocoral reefs and nanorods. The peak intensity and peak position of the UV emission were found to be different for ZnO nanostructures grown on these two substrates (Fig. 5). Two distinct peaks have been observed in both of the PL spectra, the sharp near band edge emission (NBE) and the broad deep level emission (DPE) location around 500 nm. For nanocoral reefs grown on PS substrate, a strong intensity UV peak located at 382 nm was observed. On the other hand, for nanorods grown on Si substrate, the intensity of UV peak centered at 384 nm was relatively low as compared to nanocoral reefs. The UV emission corresponds to the near band-edge emission or the recombination of free excitons through an exciton–exciton collision process [19,20]. The FWHM of the UV peak of the ZnO nanocoral reef grown on PS (14 nm) was smaller than that for the nanorods grown on Si (17 nm), indicating the better optical quality of ZnO nanocoral reefs grown at 900 °C. For the ZnO nanorods,

the UV peak appearing at 384 nm in Fig. 5 exhibited a slight shift towards lower frequency in comparison to the ZnO nanocoral reefs. The slight shift in UV emission was possible because the tensile strain became more intense as the diameter of the ZnO nanostructure increased [21]. The PL spectra of these samples show a difference in peak positions, indicating that the change in surface type influences the PL peak shift.

From Fig. 5 the PL spectrum of nanocoral reefs was observed to have a higher green emission intensity as compared to nanorods. The higher intensity of green luminescence corresponds to more oxygen vacancies and the intensity of emitted light is proportional to the number of photons emitted. This means that the number of photons emitted is much higher in the porous ZnO nanocoral reef than it is in as-grown ZnO nanorods. From the literature, the mechanism for the origination of DPE (green emission) has not been fully understood, and so far, the most reported mechanism for the presence of this green emission was attributed to the radial recombination of a photo-generated hole with electron of the singly ionized oxygen vacancies in the surface lattices of the ZnO [22]. It has also been reported that the radiative transitions between shallow donors (related to oxygen vacancies) and deep acceptors (zinc vacancies) can create defects in the luminescence spectra [23].

It has been shown that the intensity of the green emission was strongly influenced by the surface condition of the ZnO nanostructures [24,25]. Wang et al. [26], pointed out that, through the surface band bending, the chemisorbed oxygen played a crucial role in the recombination process of the green emission. Equivalently important is the concentration and the spatial distribution of the defect states, at which the recombination process of the green emission takes place. It is believed that the recombination process occurs through the transition between two defect-levels with one of them being involved in the interstitial zinc or its complex [27,28].

In this study, obviously, the PS surface provides a rough surface morphology to form a wetting layer by decreasing the surface energy, thus allowing the ZnO nanostructures to grow without any catalyst. The rough morphology of a PS surface was proven to be advantageous for the growth of nanowires by reducing its strain and increasing the number of nuclei sites [29].

4. Conclusion

In summary, we have synthesized large-scale aligned ZnO nanocoral reefs and nanorods on PS/Si and Si without the use of catalyst at 900 °C by simple oxidation of Zn powders. The dependence of the structural and optical properties of these nanostructures on the different substrates was investigated systematically. The nanostructures were polycrystalline in nature, (0 0 2) plane was the preferred orientation, and showed decreasing crystal grain size with porous silicon substrates. A strongest UV emission intensity and the narrowest FWHM for ZnO nanocoral reefs have been obtained on PS substrate compared to ZnO nanorods as grown on Si substrate. This non-catalyst growth technique on the rough surfaces of substrates may allow materials to modify the band structure and lead to unique optical properties for applications in the fabrication of nanoelectronic and nanooptical devices.

Acknowledgement

The authors would like to acknowledge financial support from the FRGS Grant and Universiti Sains Malaysia.

References

[1] C. Klingshirn, Phys. Status Solidi B 71 (1975) 547.
[2] Y.G. Wang, S.P. Lau, H.W. Lee, S.F. Yu, B.K. Tay, J. Appl. Phys. 94 (2003) 354.
[3] J.B. Webb, D.F. Williams, M. Buchanan, Appl. Phys. Lett. 39 (1981) 640.
[4] M. Bagnall, Y.F. Chen, Z. Zhu, T. Yao, S. Koyama, M.Y. Shen, T. Goto, Appl. Phys. Lett. 70 (1997) 2230.
[5] Y.S. Lee, T.Y. Tseng, J. Mater. Sci. Mater. Electron. 9 (1998) 65.
[6] H.I. Abdulgafour, Z. Hassan, N.H. Al-Hardan, F.K. Yam, Physica B 405 (2010) 4216.
[7] J.S. Lee, M.I. Kang, S. Kim, M.S. Lee, Y.K. Lee:, J. Cryst. Growth 249 (2003) 201.
[8] Y.W. Wang, L.D. Zhang, G.Z. Wang, X.S. Peng, Z.Q. Chu, C.H. Liang, J. Cryst. Growth 234 (2002) 171.
[9] Z.L. Wang, R.P. Gao, Z.W. Pan, Z.R. Dai, Adv. Eng. Mater. 3 (2001) 657.
[10] Y.L. Wang, X.C. Jiang, Y.N. Xia, J. Am. Chem. Soc. 1 (25) (2003) 16176.
[11] W.I. Park, Gyu-Chui. Yi, M.Y. Kim, S.J. Pennycook, Adv. Mater. 15 (2003) 526.
[12] (a) O. Bisia, S. Ossicinib, L. Pavesic Surf. Sci. Rep. 38 (2000) 1–126;
(b) W.Z. Li, H. Zhang, C.Y. Wang, Y. Zhang, L.W. Xu, K. Zhu, Appl. Phys. Lett. 70 (1997) 2685.
[13] P. Yang, C.M. Lieber, J. Mater. Res. 12 (1997) 2981.
[14] P.J. Cao, Y.S. Gu, H.W. Liu, F. Shen, Y.G. Wang, Q.F. Zhang, J.L. Wu, H.J. Gao, J. Mater. Res. 18 (2003) 1686.
[15] M.H. Huang, Y. Wu, H. Feick, N. Tran, E. Weber, P. Yang, Adv. Mater. 13 (2001) 113.
[16] N.H. Tran, A.J. Hartmann, R.N. Lamb, J. Phys. Chem. B 103 (1999) 4264.
[17] J. Lee, W. Gao, Z. Li, M. Hodgson, J. Metson, H. Gong, U. Pal, Appl. Phys. A 80 (2005) 1641–1646.
[18] Hong Caia, Honglie Shen, Yugang Yin, Linfeng Lu, Jiancang Shen, Zhengxia Tang, J. Phys. Chem. Solids 70 (2009) 967.
[19] Y.C. Kong, Y.B. Zhang, W. Fang, S.Q. Feng, Appl. Phys. Lett. 78 (2001) 407.
[20] A. Umar, Y.B. Hahn, Cryst. Growth Des. 8 (2008) 2741.
[21] J.S. Lee, K. Park, M.I. Kang, I.W. Park, S.W. Kim, W.K. Cho, H.S. Han, S.S. Kim, J. Cryst. Growth 254 (2003) 423.
[22] K. Vanheusdan, C.H. Seager, W.L. Warren, D.R. Tallent, J.A. Voigt, Appl. Phys. Lett. 68 (1995) 403.
[23] H.J. Egehaaf, D. Oelkrug, J. Cryst. Growth 161 (1996) 190.
[24] Y. Harada, S. Hashimoto, Phys. Rev. B 68 (2003) 045421.
[25] D. Li, Y.H. Leung, A.B. Djurišić, Z.T. Liu, M.H. Xie, S.L. Shi, S.J. Xu, W.K. Chan, Appl. Phys. Lett. 85 (2004) 1601.
[26] D. Wang, N. Sathitsuksanoh, A. Cheng, Y.H. Tzeng, H.W. Seo, C.C. Tin, M.J. Bozack, J.R. Williams, M. Park, J. Appl. Phys. 99 (2006) 113509.
[27] P.S. Xu, Y.M. Sun, C.S. Shi, F.Q. Xu, H.B. Pan, Nucl. Instrum. Methods Phys. Res. B 199 (2003) 286.
[28] N.E. Korsunska, L.V. Borkovska, B.M. Bulakh, L.Yu. Khomenkova, V.I. Kushnirenko, I.V. Markevich, J. Lumin. 733 (2003) 102.
[29] V. Lehmann, U. Gosele, Appl. Phys. Lett. 58 (1991) 856.